35th Annual International Conference of the IEEE EMBS
Osaka, Japan, 3 - 7 July, 2013

Adapting Parcellation Schemes to Study Fetal Brain Connectivity in Serial Imaging Studies

Xi Cheng, Jakob Wilm, Sharmishtaa Seshamani, Mads Fogtmann, Christopher Kroenke and Colin Studholme

***Abstract*— A crucial step in studying brain connectivity is the definition of the Regions Of Interest (ROI's) which are considered as nodes of a network graph. These ROI's identified in structural imaging reflect consistent functional regions in the anatomies being compared. However in serial studies of the developing fetal brain such functional and associated structural markers are not consistently present over time. In this study we adapt two non-atlas based parcellation schemes to study the development of connectivity networks of a fetal monkey brain using Diffusion Weighted Imaging techniques. Results demonstrate that the fetal brain network exhibits small-world characteristics and a pattern of increased cluster coefficients and decreased global efficiency. These findings may provide a route to creating a new biomarker for healthy fetal brain development.**

I. INTRODUCTION

The brain can be considered as a network of highly interconnected small regions. Therefore studying its structural connectivity can help provide a better understanding of the organization of the brain. Recently, non-invasive techniques such as diffusion-weighted MRI have been used to study structural connectivity in adults and infants which have led to the discovery of small-world characteristics of the brain [1][2]. More recently, Fan [3] studied the brain network of healthy pediatric subjects at ages of 1 month, 1 year and 2 years, and identified the development of small-world topologies in this early period of development.

An important step in these studies is the partitioning of the brain into functional regions of interest (ROI's) between which connectivity is evaluated. The adult and pediatric brain parcellation schemes focus on dividing the cortex into units that represent known functional divisions often defined in MRI by the presence of cortical folds or sulci and gyri. However in the developing fetal brain such units may not be present at a given gestational age and their structural correlates in the form of sulci and gyri are not developed. In order to study early brain growth we therefore must develop a connectivity mapping methodology that is independent of cortical folding and its rapid change over time. A very recent structural connectivity study [4] of neonatal brains used two automated methods for parcellating the brain surface, i.e., (1) the brain was partitioned using 3D regular lattice into spatial regions of equal spatial extent along the x, y, and z axes of the imaging volume, and (2) derived subcortical surface was divided based on Recursive Zonal Equal Area Sphere Partition. However, for serial studies of growth over time these approaches create partitions which can have inconsistencies in region areas as the brain grows. The first method may break regions unexpectedly and results in large differences in ROI sizes, especially when the number of ROI's increases. In addition to cortical partitioning, in the fetus we are also interested in dividing the developing cerebral mantle. Unfortunately, the second method which is basically surface projection cannot be applied here. Hagmann [5] used a two phase random parcellation method to study the adult brain structural connectivity. However the number of ROI's cannot be pre-determined in this method. This is a limitation in the case where one is interested in performing a controlled analysis of network by varying the number of nodes systematically.

Rather that assuming a specific functional and anatomical correspondence over time from which to derive connectivity measures as the brain rapidly develops, here we explore approaches that simply aim to sample that anatomical or functional pattern and its connectivity in a way that allows us to evaluate spatial connectivity as the brain grows. As with any imaging process, sampling of spatial data can be achieved using different schemes. Here we explore adaptations of regular and random sampling with the aim of ensuring consistency of anatomical sampling over time. We use animal imaging data (the Macacque monkey) as a basis for this study as it provides a high quality reference not currently available in normal human studies.

II. MATERIALS AND METHOD

A. Data Acquisition

We acquired a dataset consisting of both T2-weighted and Diffusion Weighted Imaging (DWI) data of an in-vivo monkey fetus at gestational ages of 85, 110 and 135 days from a 3T Siemens scanner. The T2-weighted data consists of 12 scans with a resolution of $0.667 \times 0.667 \times 1mm$, $TE = 97ms$, $TR = 9900ms$. The DWI data consists of 3 scans, each containing 27 stacks (9 axial, 9 sagittal and 9 coronal) with a resolution of $1.125 \times 1.125 \times 3mm$, 20 diffusion weighted directions, $b = 500s/mm^2$, $TE = 93ms$ and $TR = 5000ms$.

B. Data Preprocessing

The T2-weighted multi-slice acquisitions were motion corrected and reconstructed to isotropic 0.5mm voxels with

*This work was supported by NIH grants NIH/NINDS R01 NS 061957 and NIH/NINDS R01 NS 055064.

X. Cheng (chengxi7@uw.edu), S. Seshamani, M. Fogtmann and C. Studholme are with the Biomedical Image Computing Group, **http://depts.washington.edu/bicg**, Departments of Pediatrics and Bioengineering, University of Washington, Seattle, WA, USA.

J. Wilm is with Department of Informatics and Mathematical Modeling, Technical University of Denmark, Kongens, Lyngby, Denmark.

C. Croenke is with Department of Behavioral Neuroscience, Oregon Health & Science University, Portland, OR, USA.

978-1-4577-0216-7/13/$26.00 ©2013 IEEE

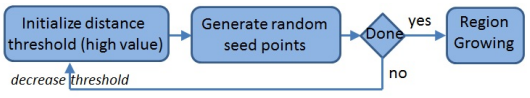

(a) random parcellation

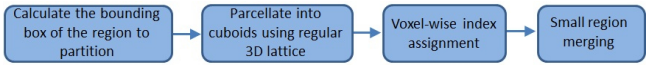

(b) regular parcellation

Fig. 1. Parcellation Algorithm Overview: different steps in (a) random parcellation, and (b) regular parcellation.

the approach described in [6]. All the DWI acquisitions were motion corrected and reconstructed to a rank 2 tensor with an isotropic spatial resolution of 0.75mm [7], which was then registered to the reconstructed T2-weighted volume and up-sampled to the same resolution as T2-weighted volume. The T2-weighted image was segmented into two basic regions: the cortical plate and cerebral mantle. The cerebral mantle here included subplate, intermediate zone, deep grey matter and germinal matrix.

C. Region Partition

We consider 2 types of parcellation schemes whose steps are shown in Fig. 1:

1) Random parcellation: A number of seed points are randomly generated within the mask followed by region growing, where all voxels in the mask are assigned to the nearest seed point. To avoid trivial ROI's whose size would be much lower than that of others, a distance threshold was used to make the random seed points well distributed when they were generated. This ensured that the distance between any pair of seed points was above the threshold. An appropriate threshold is selected by first creating the partitioning with a high value and reducing this until the required number of seed points is generated.

2) Regular parcellation: All volumes (T2-weighted, DTI and mask) were manually transformed to standardize the axial orientation and centering. A bounding box of the mask was calculated and then divided into cuboids of equal size. These cuboids were then assigned an integer index derived from their x, y, z locations in the image space. The individual image voxels within the brain mask were then assigned label values corresponding to the index of the cuboid they were in. The assignment may result in small boundary ROI's when the mask is irregular, whose connection to other ROI's can be meaningless. Therefore, ROI's whose sizes were smaller than a predefined threshold were merged into its nearest ROI recursively until the sizes of all ROI's were larger than the threshold.

Compared to the regular parcellation scheme, the random parcellation scheme has several advantages. In particular, it allows more direct control over the number of ROI's within the brain mask and avoids the creation of trivial ROI's at the brain boundary when the brain shape becomes more complex. For random parcellation, we repeated the experiments 40 times for each number of ROI's to specifically examine the consistency as the sampling of the functional regions is varied. We also varied the number of ROI's in both parcellation schemes to examine its effect on the connectivity measures. Specifically, we partitioned the cerebral mantle into ROI's of which the number varies from 60 to 140 in subcortical connectivity study. In cortical connectivity study, we partitioned the cortical plate into ROI's of which the number ranges from 30 to 65 only using the random parcellation.

D. Tractography

Whole-brain streamlined fiber tractography was performed with the deterministic Fiber Assignment by Continuous Tracking (FACT) algorithm [8], using a mask consisting of the sub-plate, cortical mantle, deep grey matter and germinal matrix segmented from the reconstructed T2-weighted volume. A maximum turning angle of 45^o, a minimum fractional anisotropy (FA) of 0.08 and a tracing step size of 0.1 voxel were chosen. This step recovers the fiber tracts in the white matter.

E. Network Graph Analysis

The unweighted connectivity network graph was constructed using the ROI's resulting from the parcellation as nodes. Two nodes are considered connected if there exists at least one fiber connecting them. The unweighed graph is also represented as an binary adjacency matrix $A_{N\times N}$, where N is the number of ROI's and $A_{ij} = 1$ if the i-th and j-th node are connected and 0 otherwise. Small-world analysis was applied to the graph which involved computing measurements of segregation (cluster coefficient) and integration (global efficiency) [9] and comparing these metrics to those of a randomized network with the same number of nodes and degree distribution. The cluster coefficient (C) and global efficiency (E) are defined as :

$$C = \frac{1}{n}\sum_{i\in N} C_i = \frac{1}{n}\sum_{i\in N}\frac{2t_i}{k_i(k_i-1)} \quad (1)$$

$$E = \frac{1}{n}\sum_{i\in N} E_i = \frac{1}{n(n-1)}\sum_{\substack{i,j\in N\\ i\neq j}}\frac{1}{d_{ij}} \quad (2)$$

where C_i is the cluster coefficient and k_i is the degree of the node i, t_i is the number of triangles formed by the neighbouring nodes of node i, E_i is the global efficiency of node i, d_{ij} is the number of nodes along the shortest path from node i to node j, n is the total number of nodes in the node set N.

Small-world networks are characterized by dense local clustering of connections between neighbouring nodes and short path lengths between any pair of nodes due to the existence of relatively few long-range connections [10]. Thus, its clustering coefficient is much larger than that of a randomized network ($C >> C_{rand}$), while its global efficiency is slightly smaller ($E < E_{rand}$).

III. RESULTS

We performed both subcortical and cortical connectivity studies on the acquired data.

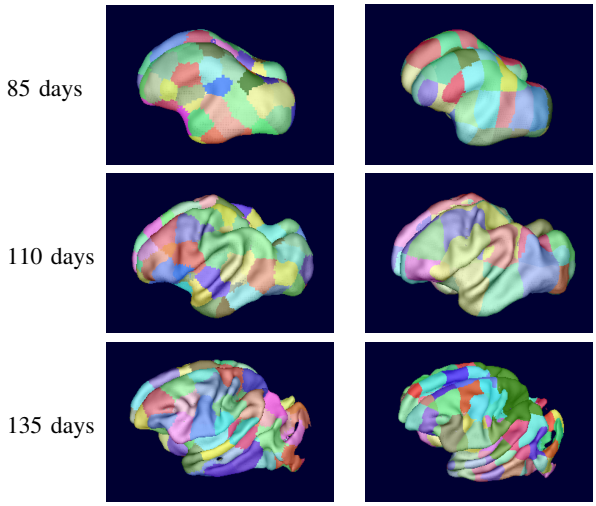

Fig. 2. 3D surface renderring of partitioned brains at all 3 time points using both random and regular parcellation schemes.

Subcortical connectivity

Fig. 2 shows an example of partitioning the same brain (cerebral mantle) at all 3 ages using both regular and random parcellation schemes. Fig. 3 shows the traced fiber tracts connecting cortical ROI's at all 3 time points, which are colored by the FA map and overlaid on the corresponding T2-weighted images. We then constructed the brain connectivity network graph for each dataset based on the ROI's and all traced fiber tracts.

We performed small-world analysis on the extracted graphs. From Fig. 4(a,b), we can see that the cluster coefficient of subcortical connectivity networks is much larger than that of the random networks while the global efficiency is slightly smaller, indicating that these networks both exhibit small-world characteristics. Both the cluster coefficient and the global efficiency increase as the brain develops. Fig. 4(c,d) indicates that these network properties are robust to parcellation schemes and different numbers of ROI's to partition. However, the number of ROI's should not be too small to better reveal the development of the fetal brain connectivity network, especially for global efficiency of the brain networks at 110 days and 135 days, when the brain is largest.

Cortical connectivity

Fig. 5 shows the results of small-world analysis of the cortical connectivity network. We can observe that the cortical connectivity network also exhibits small-world characteristics. Besides, the cluster coefficient and global efficiency increase across brain development. These results are also robust to the number of ROI's in the experimental range.

IV. DISCUSSION

The results of cortical and subcortical connectivity networks both identified small-world characteristics of the fetal brain network. This suggests that the characteristics of brain network have been selected to solve the problem of optimizing the brain information processing since its very early development stage. Besides, the studies also demonstrated a pattern of increased cluster coefficients as well as global efficiency, meaning the overall efficiency of the brain in processing information increases during its maturation. These observations parallel the fact that myelination is in progress and only partially formed at birth [11]. Furthermore, the robustness of these results to the number of ROI's indicates the feasibility of applying small-world analysis to studying developing fetal brains which is undergoing considerable size and shape changes. Another observation from the small-world analysis is that the cluster coefficients of the brain network decrease linearly as the number of ROI's increases, however the cluster coefficients of the random network seem to decrease quadratically, as shown in Fig. 4(a) and Fig. 5. This could potentially be useful in predicting abnormalities in fetal brain connectivity.

In conclusion, we have studied the changes in structural connectivity networks in the monkey fetal brain using unbiased random and regular parcellation schemes and graph theory based analysis. The findings provide a picture of the development of fetal brain networks, complementing the existing studies in adult and baby brain networks. Future work will explore the use of these measures in normal human development and their use in studying and quantifying abnormal connectivity [12].

REFERENCES

[1] Y. Iturria-Medina, R. C. Sotero, E. J. Canales-Rodríguez, Y. Alemán-Gómez, and L. Melie-García, "Studying the human brain anatomical network via diffusion-weighted MRI and graph theory," *NeuroImage*, vol. 40, pp. 1064–1076, 2008.

[2] G. Gong, Y. He, L. Concha, C. Lebel, D. W. Gross, A. C. Evans, and C. Beaulieu, "Mapping anatomical connectivity patterns of human cerebral cortex using in vivo diffusion tensor imaging tractography," *Cerabral Cortex Match*, vol. 19, pp. 524–536, 2009.

[3] Y. Fan, F. Shi, J. K. Smith, W. Lin, J. H. Gilmore, and D. Shen, "Brain anatomical networks in early human brain development," *NeuroImage*, vol. 54, pp. 1862–1871, 2009.

[4] O. Tymofiyeva1, C. P. Hess, E. Ziv, N. Tian, S. L. Bonifacio, P. S. McQuillen, D. M. Ferriero, A. J. Barkovich1, and D. Xu, "Baby connectome: Mapping the structural connectivity of the newborn brain," *NeuroImage*, vol. 52, pp. 1059–1069, 2010.

[5] P. Hagmann, M. Kurant, X. Gigandet, P. Thiran, V. J. Wedeen, R. Meuli, and J.-P. Thiran, "Mapping human whole-brain structural networks with diffusion MRI," *PLoS ONE*, vol. 2, no. 7, p. e597, 2007.

[6] M. Fogtmann, T. Chapman, K. Kim, S. Seshamani, and C. Studholme, "A unified approach for motion-estimation and super-resolution reconstruction from structural magnetic resonance on moving subjects," in *MICCAI Workshop on Perinatal and Paediatric Imaging*, Nice, France, Oct. 2012.

[7] M. Fogtmann, S. Seshamani, C. Kroenke, T. Chapman, J. Wilm, F. Rousseau, M. Koob, J.-L. Dietemann, and C. Studholme, "A unified approach to diffusion direction sensitive slice registration and 3D DTI reconstruction from moving fetal brain anatomy," *IEEE Trans. Med. Imaging*, submitted for publication.

[8] S. Mori and P. C. M. van Zijl, "Fiber tracking: principles and strategies - a technical review," *NMI IN BIOMEDICINE*, vol. 15, pp. 468–480, 2002.

[9] M. Rubinov and O. Sporns, "Complex network measures of brain connectivity: Uses and interpretations," *NeuroImage*, vol. 52, pp. 1059–1069, 2010.

[10] D. S. Bassett and E. Bullmore, "Small-world brain networks," *The Neuroscientist*, vol. 12, no. 6, pp. 512–523, 2006.

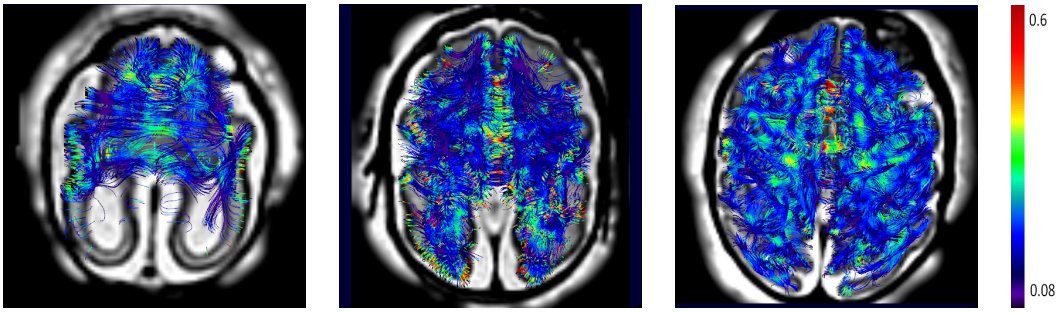

(a) 85 days (b) 110 days (c) 135 days

Fig. 3. All fiber tracts connecting cortical ROI's traced at all 3 time points. The fibers are overlaid on T2W structural images and colored by FA map.

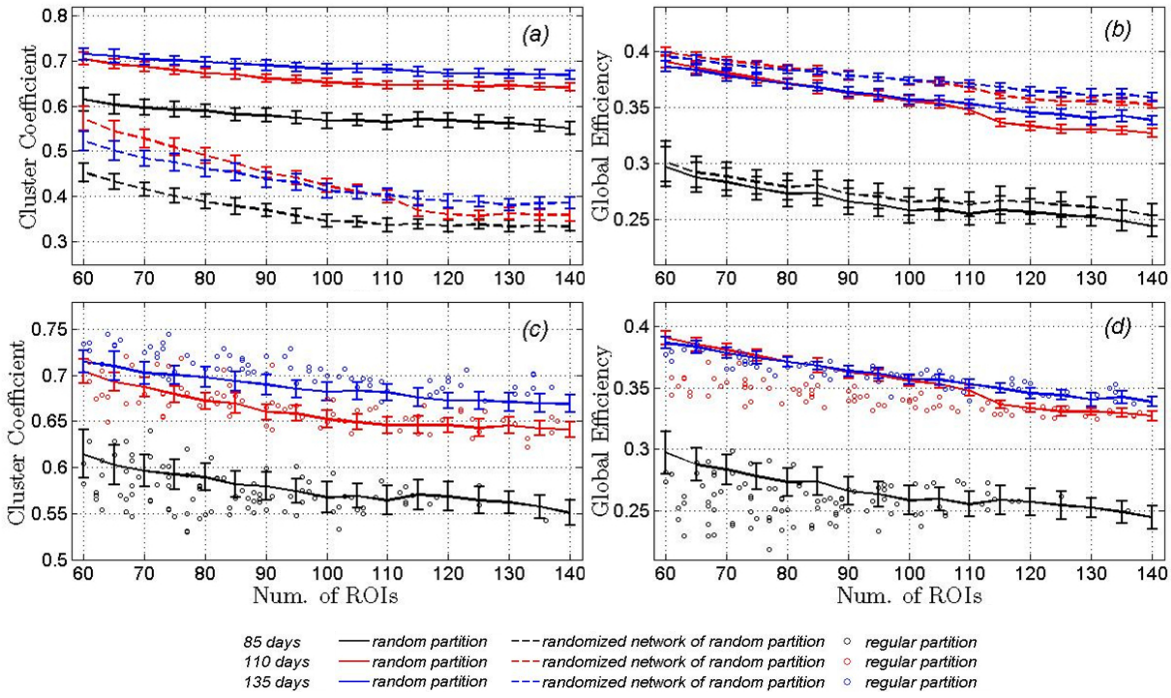

Fig. 4. Subcortical connectivity: cluster coefficient and global efficiency (mean±standard deviation) as a function of the number of nodes at all 3 ages. (a,b) compare these measurements of random partition based brain network and random network for testing the small-worldness of subcortical brain networks. (c,d) compare the measurements obtained from both random and regular partition methods.

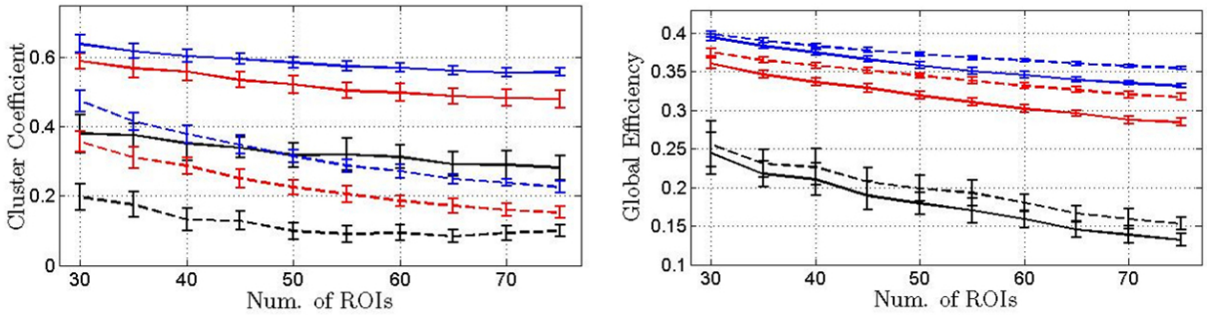

Fig. 5. Cortical connectivity: cluster coefficient and global efficiency (mean±standard deviation) as a function of the number of nodes based on random partition scheme at all 3 ages. These measurements of random graphs are also plotted as dashed lines for testing the small-worldness of cortical brain networks. *For legend see Fig. 4*.

[11] R. D. Fields, "White matter matters," *Scientific American*, vol. 298, pp. 54–61, 2008.

[12] M. Koob, A. sophie Weingertner, B. Gasser, E. Oubel, and J.-L. Dietemann, "Thick corpus callosum: a clue to the diagnosis of fetal septopreoptic holoprosencephaly?" *Pediatr Radiol*, vol. 42, no. 7, pp. 886–890, 2011.